A new gravitational wave background from the Big Bang

Juan García-Bellido[1] and Daniel G. Figueroa[2]

Instituto de Física Teórica CSIC-UAM,
Universidad Autónoma de Madrid,
Cantoblanco 28049 Madrid, Spain

Abstract

The reheating of the universe after hybrid inflation proceeds through the nucleation and subsequent collision of large concentrations of energy density in the form of bubble-like structures moving at relativistic speeds. This generates a significant fraction of energy in the form of a stochastic background of gravitational waves, whose time evolution is determined by the successive stages of reheating: First, tachyonic preheating makes the amplitude of gravity waves grow exponentially fast. Second, bubble collisions add a new burst of gravitational radiation. Third, turbulent motions finally sets the end of gravitational waves production. From then on, these waves propagate unimpeded to us. We find that the fraction of energy density today in these primordial gravitational waves could be significant for GUT-scale models of inflation, although well beyond the frequency range sensitivity of gravitational wave observatories like LIGO, LISA or BBO. However, low-scale models could still produce a detectable signal at frequencies accessible to BBO or DECIGO. For comparison, we have also computed the analogous background from some chaotic inflation models and obtained similar results to those of other groups. The discovery of such a background would open a new observational window into the very early universe, where the details of the process of reheating, i.e. the Big Bang, could be explored. Thus, it could also serve as a new experimental tool for testing the Inflationary Paradigm.

1   Introduction

Gravitational waves (GW) are ripples in space-time that travel at the speed of light, and whose emission by relativistic bodies represents a robust prediction of General Relativity. Theoretically, it is expected that the present universe should be permeated by a diffuse background of GW of either an astrophysical or cosmological origin [1]. Fortunately, these backgrounds have very different spectral signatures that might, in the future, allow gravitational wave observatories like LIGO [2], LISA [3], BBO [4] or DECIGO [5], to disentangle their origin [1]. Unfortunately, the weakness of gravity will make this task extremely difficult, requiring a very high accuracy in order to distinguish one background from another.

There are, indeed, a series of constraints on some of these backgrounds, coming from the anisotropies in the Cosmic Microwave Background (CMB) [6], from Big Bang nucleosynthesis [7] or from millisecond pulsar timing [8]. Most of these constraints come at very low frequencies, from 10^{-18} Hz to 10^{-8} Hz, while present and future GW detectors (will) work at frequencies of order $10^{-3} - 10^3$ Hz. If early universe first order phase transitions [9, 10] or cosmic turbulence [11] occurred around the electro-weak (EW) scale, GW detectors could have a chance to measure the corresponding associated backgrounds. However, if those processes occurred at the GUT scale, their corresponding backgrounds will go undetected by the actual detectors, since these cannot reach the required sensitivity in the high frequency range of $10^7 - 10^9$ Hz. There are however recent proposals to cover this range [12, 13], which may become competitive in the not so far future.

---

[1]E-mail: juan.garciabellido@uam.es
[2]E-mail: daniel.figueroa@uam.es

Cosmological observations seem to suggest that something like Inflation must have occurred in the very early universe. Approximately scale-invariant density perturbations, sourced by quantum fluctuations during inflation, seem to be the most satisfying explanation for the CMB anisotropies. Together with such scalar perturbations one also expects tensor perturbations (GW) to be produced, with an almost scale-free power spectrum [14]. The detection of such a background is crucial for early universe cosmology because it would help to determine the absolute energy scale of inflation, a quantity that for the moment is still uncertain, and would open the exploration of physics at very high energies.

However, in the early universe, after inflation, other GWB could have been produced at shorter wavelengths, in a more 'classical' manner rather than sourced by quantum fluctuations. In particular, whenever there are large and fast moving inhomogeneities in a matter distribution, one expects the emission of GW. At large distances from a source, the amplitude of the GW is given by $h_{ij} \simeq G\ddot{Q}_{ij}/c^4 r$, with Q_{ij} the quadrupole moment of the mass distribution. The larger the velocity of the matter distribution, the larger the amplitude of the radiation produced. However, because of the weakness of gravity, in order to produce a significant amount of gravitational radiation, it is required a very relativistic motion (and high density contrasts) in the matter distribution of a source. Fortunately, this is indeed believed to be the situation at the end of inflaton, during the conversion of the huge energy density driving inflation into radiation and matter, at the so-called *reheating* of the Universe [15], i.e. at the Big Bang.

Note that any background of GW coming from the early universe, if generated below Planck scale, immediately decoupled upon production and, whatever their spectral signatures, they will retain their shape throughout the expansion of the Universe. Thus, the characteristic frequency and shape of the GWB generated at a given time should contain information about the very early state of the Universe in which it was produced. Actually, it is conceivable that, in the not so far future, the detection of these GW backgrounds could be the only way we may have to infer the physical conditions of the Universe at such high energy scales. However, the same reason that makes GW ideal probes of the early universe − the weakness of gravity − is responsible for the extreme difficulties we have for their detection on Earth.

In Refs. [16, 17] we described the stochastic background predicted to arise from reheating after hybrid inflation. Here we will review the various processes involved in the production of such a background. In the future, this background could serve as a new tool to discriminate among different inflationary models, since reheating in each model would give rise to a different GWB with very characteristic spectral features. The details of the dynamics of preheating depend very much on the model and are often very complicated because of the non-linear, non-perturbative and out-of-equilibrium character of the process itself. However, all the cases have in common that only specific resonance bands of the fields suffer an exponential instability, which makes their occupation numbers grow by many orders of magnitude. The shape and size of the spectral bands depend very much on the inflationary model. If one translates this picture into position-space, the highly populated modes correspond to large time-dependent inhomogeneities in the matter distributions which acts, in fact, as a powerful source of GW. For example, in single field chaotic inflation models, the coherent oscillations of the inflaton during preheating generates, via parametric resonance, a population of highly occupied modes that behave like waves of matter. They collide among themselves and their scattering leads to homogenization and local thermal equilibrium. These collisions occur in a highly relativistic and very asymmetric way, being responsible for the generation of a stochastic GWB [18, 19, 20, 21, 22] with a typical frequency today of the order of $10^7 - 10^9$ Hz, corresponding to the present size of the causal horizon at the end of high-scale inflation.

However, there are models like hybrid inflation in which the end of inflation is sudden [23] and the conversion into radiation occurs almost instantaneously. Indeed, hybrid models preheat very violently, via the spinodal instability of the symmetry breaking field that triggers the end of inflation, irrespective of the couplings that this field may have to the rest of matter. Such a process is known as *tachyonic preheating* [24, 25] and could be responsible for copious production of dark matter particles [26], lepto and baryogenesis [27], topological defects [24], primordial magnetic fields [28], etc. In Ref. [25], it was shown that the process of symmetry breaking in hybrid preheating, proceeds via the nucleation of dense bubble-like structures moving at relativistic speeds, which collide and break up into smaller structures (see Figs. 7 and 8 of Ref. [25]). We conjectured at that time that such collisions would be a very strong source of GW, analogous to the GW production associated with strongly first order phase transitions [9]. As we will show here, this is indeed the case during the nucleation, collision and subsequent rescattering of the initial bubble-like structures produced after hybrid inflation. During the different stages of reheating

in this model, gravity waves are generated and amplified until the Universe finally thermalizes and enters into the radiation era of the Standard Model of Cosmology. From that moment until now, this cosmic GWB will be redshifted as a radiation-like fluid, totally decoupled from any other energy-matter content of the universe, such that today's ratio of energy stored in these GW to that in radiation, could range from $\Omega_{\mathrm{GW}} h^2 \sim 10^{-8}$, peacked around $f \sim 10^7$ Hz for the high-scale models, to $\Omega_{\mathrm{GW}} h^2 \sim 10^{-11}$, peacked around $f \sim 1$ Hz for the low-scale models.

Finally, since the first paper by Khlebnikov and Tkachev [18], studing the GWB produced at reheating after chaotic inflation, there has been some developments. The idea was soon extended to hybrid inflation in Ref. [19]. It was also revisited very recently in Ref. [20, 21] for the $\lambda\phi^4$ and $m^2\phi^2$ chaotic scenarios, and reanalysed again for hybrid inflation in Refs. [16, 17], using the new formalism of tachyonic preheating [24, 25]. Because of the increase in computer power of the last few years, we are now able to perform precise simulations of the reheating process in a reasonable time scale. Moreover, understanding of reheating has improved, while gravitational waves detectors are beginning to attain the aimed sensitivity [2]. Furthermore, since these cosmic GWBs could serve as a deep probe into the very early universe, we should characterize in the most detailed way the information that we will be able to extract from them.

2   Gravitational Wave Production

Our main purpose here is to study the details of the stochastic GWB produced during the reheating stage after hybrid inflation (sections 2 and 3). Nevertheless, we also study more briefly the analogous background from reheating in some chaotic models (section 4). Thus, in this section we derive a general formalism for extracting the GW power spectrum in any scenario of reheating within the (flat) Friedman-Robertson-Walker (FRW) universe. The formalism will be simplified when applied to scenarios in which we can neglect the expansion of the universe, like in the case of Hybrid models.

A theory with an inflaton scalar field χ interacting with other Bose fields ϕ_a, can be described by

$$\mathcal{L} = \frac{1}{2}\partial_\mu\chi\partial^\mu\chi + \frac{1}{2}\partial_\mu\phi_a\partial^\mu\phi_a + \frac{R}{16\pi G} - V(\phi,\chi) \tag{1}$$

with R the Ricci scalar. For hybrid models, we consider a generic symmetry breaking 'Higgs' field Φ, with N_c real components. We can take $\Phi^\dagger\Phi = \frac{1}{2}\sum_a \phi_a^2 \equiv |\phi|^2/2$, with a running for the number of Higgs' components, e.g. $N_c = 1$ for a real scalar Higgs, $N_c = 2$ for a complex scalar Higgs or $N_c = 4$ for a $SU(2)$ Higgs, etc. The effective potential then becomes

$$V(\phi,\chi) = \frac{\lambda}{4}\left(|\phi|^2 - v^2\right)^2 + g^2\chi^2|\phi|^2 + \frac{1}{2}\mu^2\chi^2. \tag{2}$$

For chaotic scenarios, we consider a massless scalar field ϕ interacting with the inflaton χ via

$$V(\chi,\phi) = \frac{1}{2}g^2\chi^2\phi^2 + V(\chi), \tag{3}$$

with $V(\chi)$ the inflaton's potential. Concerning the simulations we show in this paper, we concentrate in the $N_c = 4$ case for the hybrid model and consider a potential $V(\chi) = \frac{\lambda}{4}\chi^4$ for the chaotic scenario.

The classical equations of motion of the inflaton and the other Bose fields are

$$\ddot{\chi} + 3H\dot{\chi} - \frac{1}{a^2}\nabla^2\chi + \frac{\partial V}{\partial\chi} = 0, \qquad \ddot{\phi}_a + 3H\dot{\phi}_a - \frac{1}{a^2}\nabla^2\phi_a + \frac{\partial V}{\partial\phi_a} = 0 \tag{4}$$

with $H = \dot{a}/a$. On the other hand, GW are represented here by a transverse-traceless (TT) gauge-invariant metric perturbation, h_{ij}, on top of the flat FRW space $ds^2 = -dt^2 + a^2(t)\left(\delta_{ij} + h_{ij}\right)dx^i dx^j$, with $a(t)$ the scale factor and the tensor perturbations verifying $\partial_i h_{ij} = h_{ii} = 0$. Then, the Einstein field equations can be splitted into the background and the perturbed equations. The former describe the evolution of the flat FRW universe through

$$-\frac{\dot{H}}{4\pi G} = \dot{\chi}^2 + \frac{1}{3a^2}(\nabla\chi)^2 + \dot{\phi}_a^2 + \frac{1}{3a^2}(\nabla\phi_a)^2 \tag{5}$$

$$\frac{3H^2}{4\pi G} = \dot{\chi}^2 + \frac{1}{a^2}(\nabla\chi)^2 + \dot{\phi}_a^2 + \frac{1}{a^2}(\nabla\phi_a)^2 + 2V(\chi,\phi) \tag{6}$$

3

where any term in the r.h.s. of (5) and (6), should be understood as spatially averaged.

On the other hand, the perturbed Einstein equations describe the evolution of the tensor perturbations [35] as

$$\ddot{h}_{ij} + 3H\dot{h}_{ij} - \frac{1}{a^2}\nabla^2 h_{ij} = 16\pi G\,\Pi_{ij}\,, \tag{7}$$

with $\partial_i\Pi_{ij} = \Pi_{ii} = 0$. The source of the GW, Π_{ij}, contributed by both the inflaton and the other scalar fields, will be just the transverse-traceless part of the (spatial-spatial) components of the total anisotropic stress-tensor

$$\mathrm{T}_{\mu\nu} = \left[\partial_\mu\chi\partial_\nu\chi + \partial_\mu\phi_a\partial_\nu\phi_a + g_{\mu\nu}(\mathcal{L} - \langle p\rangle)\right]/a^2, \tag{8}$$

where $\mathcal{L}(\chi, \phi_a)$ is the lagrangian (1) and $\langle p\rangle$ is the background homogeneous pressure. As we will explain in the next subsection, when extracting the TT part of (8), the term proportional to $g_{\mu\nu}$ in the r.h.s of (8), will be dropped out from the GW equations of motion. Thus, the effective source of the GW will be just given by the TT part of the gradient terms $\partial_\mu\chi\partial_\nu\chi + \partial_\mu\phi_a\partial_\nu\phi_a$.

2.1 The Transverse-Traceless Gauge

A generic (spatial-spatial) metric perturbation δh_{ij} has six independent degrees of freedom, whose contributions can be split into [35] scalar, vector and tensor metric perturbations $\delta h_{ij} = \psi\,\delta_{ij} + E_{,ij} + F_{(i,j)} + h_{ij}$, with $\partial_i F_i = 0$ and $\partial_i h_{ij} = h_{ii} = 0$. By choosing a transverse-traceless stress-tensor source Π_{ij}, we can eliminate all the degrees of freedom (d.o.f.) but the pure TT part, h_{ij}, which represent the only physical d.o.f which propagate and carry energy out of the source (i.e. GW). Thus, taking the TT part of the anisotropic stress-tensor, we ensure that we only source the physical d.o.f. that represent GW.

Let us switch to Fourier space. The GW equations (7) then read

$$\ddot{h}_{ij}(t, \mathbf{k}) + 3H\dot{h}_{ij}(t, \mathbf{k}) + \frac{k^2}{a^2}h_{ij}(t, \mathbf{k}) = 16\pi G\,\Pi_{ij}(t, \mathbf{k})\,, \tag{9}$$

where $k = |\mathbf{k}|$. Assuming no GW at the beginnig of reheating (i.e. the end of inflation t_e), the initial conditions are $h_{ij}(t_e) = \dot{h}_{ij}(t_e) = 0$, so the solution to Eq. (9) for $t > t_e$ will be just given by a causal convolution with an appropriate Green's function $G(t, t')$,

$$h_{ij}(t, \mathbf{k}) = 16\pi G \int_{t_e}^t dt'\, G(t, t')\Pi_{ij}(t', \mathbf{k})\,. \tag{10}$$

Therefore, all we need to know for computing the GW is the TT part of the stress-tensor, Π_{ij}, and the Green's function $G(t', t)$. However, as we will demonstrate shortly, we have used a numerical method by which we don't even need to know the actual form of $G(t', t)$. To see this, let us extract the TT part of the total stress-tensor. Given the symmetric anisotropic stress-tensor $\mathrm{T}_{\mu\nu}$ (8), we can easily obtain the TT part of its spatial components in momentum space, $\Pi_{ij}(\mathbf{k})$. Using the spatial projection operators $P_{ij} = \delta_{ij} - \hat{k}_i\hat{k}_j$, with $\hat{k}_i = k_i/k$, then [36] $\Pi_{ij}(\mathbf{k}) = \Lambda_{ij,lm}(\hat{\mathbf{k}})\mathrm{T}_{lm}(\mathbf{k})$, where

$$\Lambda_{ij,lm}(\hat{\mathbf{k}}) \equiv \left(P_{il}(\hat{\mathbf{k}})P_{jm}(\hat{\mathbf{k}}) - \frac{1}{2}P_{ij}(\hat{\mathbf{k}})P_{lm}(\hat{\mathbf{k}})\right). \tag{11}$$

Thus, one can easily see that, at any time t, $k_i\Pi_{ij}(\hat{\mathbf{k}}, t) = \Pi_i^i(\hat{\mathbf{k}}, t) = 0$, as required, thanks to the identities $P_{ij}\hat{k}_j = 0$ and $P_{ij}P_{jm} = P_{im}$.

Note that the solution (10) is just linear of the non-traceless nor-transverse tensor T_{ij} (8). Therefore, we can write the TT tensor perturbations (i.e. the GW) as

$$h_{ij}(t, \mathbf{k}) = \Lambda_{ij,lm}(\hat{\mathbf{k}})u_{lm}(t, \mathbf{k}), \tag{12}$$

with $u_{ij}(t, \mathbf{k})$ the Fourier transform of the solution of the following equation

$$\ddot{u}_{ij} + 3H\dot{u}_{ij} - \frac{1}{a^2}\nabla^2 u_{ij} = 16\pi G\,\mathrm{T}_{ij}\,. \tag{13}$$

4

This Eq. (13) is nothing but Eq. (7), sourced with the complete T_{ij} (8), instead of with its TT part, Π_{ij}. Of course, Eq. (13) contains unphysical (gauge) d.o.f.; however, in order to obtain the real physical TT d.o.f. h_{ij}, we can evolve Eq.(13) in configuration space, Fourier transform its solution and apply the projector (11) as in (12). This way we can obtain in momentum space, at any moment of the evolution, the physical TT d.o.f. that represent GW, h_{ij}. Whenever needed, we can Fourier transform back to configuration space and obtain the spatial distribution of the gravitational waves.

Moreover, since the second term of the r.h.s of the total stress-tensor T_{ij} is proportional to $g_{ij} = \delta_{ij} + h_{ij}$, see (8), when aplying the TT projector (11), the part with the δ_{ij} just drops out, simply because it is a pure trace, while the other part contributes with a term $-(\mathcal{L} - \langle p \rangle)h_{ij}$ in the l.h.s of Eq.(9). However, $(\mathcal{L} - \langle p \rangle)$ is of the same order as the metric perturbation $\sim \mathcal{O}(h)$, so this extra term is second order in the gravitational coupling and it can be neglected in the GW Eqs. (9). This way, the effective source in Eq. (13) is just the gradient terms of both the inflaton and the other scalar fields,

$$T_{ij} = (\nabla_i \chi \nabla_j \chi + \nabla_i \phi_a \nabla_j \phi_a)/a^2. \tag{14}$$

Therefore, the effective source of the physical GW, will be just the TT part of (14), as we had already mentioned before.

We have found the *commuting procedure* proposed (i.e. the fact that we first solve Eq. (13) and secondly we apply the TT projector to the solution (12), and not the other way around), very useful. We are able to extract the spectra or the spatial distribution of the GW at any desired time, saving a great amount of computing time since we don't have to be Fourier transforming the source at each time step. Most importantly, with this procedure we can take into account backreaction simultaneously with the fields evolution.

In summary, for solving the dynamics of reheating of a particular inflationary model, we evolve Eqs. (4) in the lattice, together with Eqs. (5)-(6), while for the GWs we solve Eq. (13). Then, only when required, we Fourier transform the solution of Eq. (13) and then apply (12) in order to recover the physical transverse-traceless d.o.f representing the GW. From there, one can easily build the GW spectra or take a snapshot of spatial distribution of the gravitational waves.

2.2 The energy density in GW

The energy-momentum tensor of the GW is given by [36]

$$t_{\mu\nu} = \frac{1}{32\pi G} \left\langle \partial_\mu h_{ij} \, \partial_\nu h^{ij} \right\rangle_{\mathrm{V}}, \tag{15}$$

where h_{ij} are the TT tensor perturbations solution of Eq. (7). The expectation value $\langle ... \rangle_{\mathrm{V}}$ is taken over a region of sufficiently large volume $V = L^3$ to encompass enough physical curvature to have a gauge-invariant measure of the GW energy-momentum tensor.

The GW energy density will be just $\rho_{\mathrm{GW}} = t_{00}$, so

$$\rho_{\mathrm{GW}} = \frac{1}{32\pi G} \frac{1}{L^3} \int d^3\mathbf{x} \, \dot{h}_{ij}(t,\mathbf{x}) \dot{h}_{ij}(t,\mathbf{x}) = \frac{1}{32\pi G} \frac{1}{L^3} \int d^3\mathbf{k} \, \dot{h}_{ij}(t,\mathbf{k}) \dot{h}_{ij}^*(t,\mathbf{k}), \tag{16}$$

where in the last step we Fourier transformed each $\dot{h}_{ij}$ and used the definition of the Dirac delta. We can always write the scalar product in (16) in terms of the (Fourier transformed) solution u_{lm} of the Eq.(13), by just using the fact that $\Lambda_{ij,lm}\Lambda_{lm,rs} = \Lambda_{ij,rs}$. This way, we can express the GW energy density as

$$\rho_{\mathrm{GW}} = \frac{1}{32\pi G L^3} \int k^2 dk \int d\Omega \, \Lambda_{ij,lm}(\hat{\mathbf{k}}) \dot{u}_{ij}(t,\mathbf{k}) \dot{u}_{lm}^*(t,\mathbf{k}). \tag{17}$$

From here, we can also compute the power spectrum per logarithmic frequency interval in GW, normalized to the critical density ρ_c, as $\Omega_{\mathrm{GW}} = \int \frac{df}{f} \Omega_{\mathrm{GW}}(f)$, where

$$\Omega_{\mathrm{GW}}(k) \equiv \frac{1}{\rho_c} \frac{d\rho_{\mathrm{GW}}}{d\log k} = \frac{k^3}{32\pi G L^3 \rho_c} \int d\Omega \, \Lambda_{ij,lm}(\hat{\mathbf{k}}) \dot{u}_{ij}(t,\mathbf{k}) \dot{u}_{lm}^*(t,\mathbf{k}) \tag{18}$$

We have checked explicitly in the simulations that the argument of the angular integral of (18) is independent of the directions in $\mathbf{k}$-space. Thus, whenever we plot the GW spectrum of any model, we

will be showing the amplitude of the spectrum (per each mode k) as obtained after avaraging over all the directions in momentum space,

$$\Omega_{\mathrm{GW}}(k) = \frac{k^3}{8GL^3\rho_c} \left\langle \Lambda_{ij,lm}(\hat{\mathbf{k}})\dot{u}_{ij}(t,\mathbf{k})\dot{u}_{lm}^*(t,\mathbf{k}) \right\rangle_{4\pi} \tag{19}$$

with $\langle f \rangle_{4\pi} \equiv \frac{1}{4\pi} \int f \mathrm{d}\Omega$.

Finally, we must address the fact that the frequency range, for a GWB produced in the early universe, will be redshifted today. We should calculate the characteristic physical wavenumber of the present GW spectrum, which is redshifted from any time t during GW production. So let us distinguish four characteristic times: the end of inflation, t_e; the time t_* when GW production stops; the time t_r when the universe finally reheats and enters into the radiation era; and today, t_0. Thus, today's frequency f_0 is related to the physical wavenumber k_t at any time t of GW production, via $f_0 = (a_t/a_0)(k_t/2\pi)$, with a_0 and a_t, the scale factor today and at the time t, respectively. Thermal equilibrium was established at some temperature T_r, at time $t_r \geq t$. The Hubble rate at that time was $M_P^2 H_r^2 = (8\pi/3)\rho_r$, with $\rho_r = g_r\pi^2 T_r^4/30$ the relativistic energy density and g_r the effective number of relativistic degrees of freedom at temperature T_r. Since then, the scale factor has increased as $a_r/a_0 = (g_{0,s}/g_{r,s})^{1/3}(T_0/T_r)$, with $g_{i,s}$ the effective entropic degrees of freedom at time t_i, and T_0 today's CMB temperature. Putting all together,

$$f_0 = \left(\frac{8\pi^3 g_r}{90}\right)^{\frac{1}{4}} \left(\frac{g_{0,s}}{g_{r,s}}\right)^{\frac{1}{3}} \frac{T_0}{\sqrt{H_r M_p}} \left(\frac{a_e}{a_r}\right) \frac{k}{2\pi} \,, \tag{20}$$

where we have used the fact that the physical wave number k_t at any time t during GW production, is related to the comoving wavenumber k through $k_t = (a_e/a_t)k$ with the normalization $a_e \equiv 1$.

From now on, we will be concerned with hybrid inflation, leaving chaotic inflation for section 4. Within the hybrid scenario, we will analyse the dependence of the shape and amplitude of the produced GWB on the scale of hybrid inflation, and more specifically on the *v.e.v.* of the Higgs field triggering the end of inflation. Given the natural frequency at hand in hybrid models, $m = \sqrt{\lambda}v$, whose inverse m^{-1} sets the characteristic time scale during the first stages of reheating, it happens that as long as $v \ll M_p$, the Hubble rate $H \sim \sqrt{\lambda}(v^2/M_p)$ is much smaller than such a frequency, $H \ll m$. Indeed, all the initial vacuum energy ρ_0 gets typically converted into radiation in less than a Hubble time, in just a few m^{-1} time steps. Therefore, we should be able to ignore the dilution due to the expansion of the universe during the production of GW, at least during the first stages of reheating. Our approach will be to ignore the expansion of the Universe, such that we fix the scale factor to one, $a = 1$. As we will see later, neglecting the expansion of the Universe for the time of GW production, will be completely justified *a posteriori*.

The system of equations that we have to solve numerically in a lattice for the hybrid model are

$$\ddot{u}_{ij} - \nabla^2 u_{ij} = 16\pi G\, \mathrm{T}_{ij} \tag{21}$$

$$\ddot{\chi} - \nabla^2 \chi + \left(g^2|\phi|^2 + \mu^2\right)\chi = 0 \tag{22}$$

$$\ddot{\phi}_a - \nabla^2 \phi_a + \left(g^2\chi^2 + \lambda|\phi|^2 - m^2\right)\phi_a = 0 \tag{23}$$

with T_{ij} given by Eq.(14) with the scale factor $a = 1$. We have explicitly checked in our computer simulations that the backreaction of the gravity waves into the dynamics of both the inflaton and the Higgs fields is negligible and can be safely ignored. We thus omit the backreaction terms in the above equations.

We evaluated during the evolution of the system the mean field values, as well as the different energy components. Initially, the Higgs field grows towards the true vacuum and the inflaton moves towards the minimum of its potential and oscillates around it. We have checked that the sum of the averaged gradient, kinetic and potential energies (contributed by both the inflaton and the Higgs), remains constant during reheating, as expected, since the expansion of the universe is irrelevant in this model. We have also checked that the time evolution of the different energy components is the same for different lattices, changing the number of points N, the minimum momentum $p_{\min} = 2\pi/L$ or the lattice spacing $a = L/N$, with L the lattice size. The evolution of the Higgs' *v.e.v.* follows three stages easily distinguished. First, an exponential growth of the *v.e.v.* towards the true vacuum. This is driven by the tachyonic instability of the long-wave modes of the Higgs field, that makes the spatial distribution of this field to form lumps and
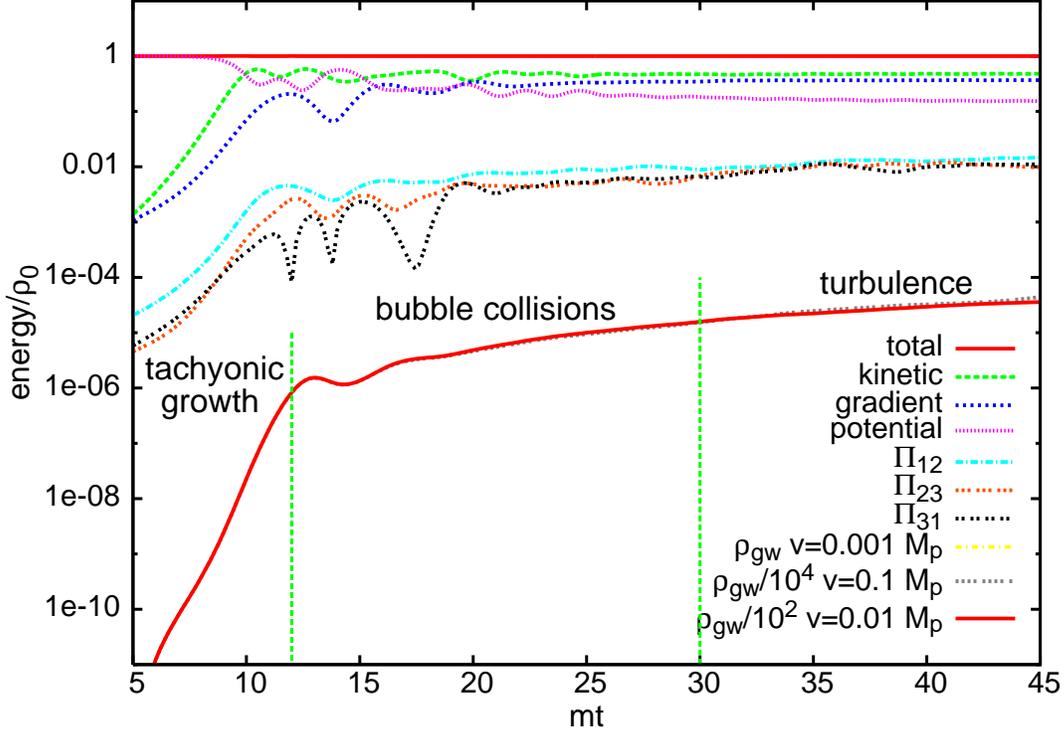
Figure 1: The time evolution of the different types of energy (kinetic, gradient, potential, anisotropic components and gravitational waves for different lattices), normalized to the initial vacuum energy, after hybrid inflation, for a model with $v = 10^{-3} M_P$. One can clearly distinguish here three stages: tachyonic growth, bubble collisions and turbulence.

bubble-like structures [24, 25]. Second, the Higgs field oscillates around the true vacuum, as the Higgs' bubbles collide and scatter off eachother. Third, a period of turbulence is reached, during which the inflaton oscillates around its minimum and the Higgs sits in the true vacuum. For a detailed description of the dynamics of these fields see Ref. [25]. Here we will be only concerned with the details of the gravitational wave production.

The initial energy density at the end of hybrid inflation is given by $\rho_0 = m^2 v^2/4$, with $m^2 = \lambda v^2$, so the fractional energy density in gravitational waves is

$$\frac{\rho_{\rm GW}}{\rho_0} = \frac{4 t_{00}}{v^2 m^2} = \frac{1}{8\pi\, G v^2 m^2} \left\langle \dot{h}_{ij} \dot{h}^{ij} \right\rangle_{\rm V} , \tag{24}$$

where $\left\langle \dot{h}_{ij} \dot{h}^{ij} \right\rangle_V$, defined as a volume average like $\frac{1}{V} \int d^3\mathbf{x} \dot{h}_{ij} \dot{h}^{ij}$, is extracted from the simulations as

$$\left\langle \dot{h}_{ij} \dot{h}^{ij} \right\rangle_{\rm V} = \frac{4\pi}{V} \int d\log k\, k^3 \left\langle \Lambda_{ij,lm}(\hat{\mathbf{k}}) \dot{u}_{ij}(t, \mathbf{k}) \dot{u}^*_{lm}(t, \mathbf{k}) \right\rangle_{4\pi} \tag{25}$$

where $u_{ij}(t, \mathbf{k})$ is the Fourier transform of the solution of Eq. (21). Then, we can compute the corresponding density parameter today (with $\Omega_{\rm rad} h^2 \simeq 3.5 \times 10^{-5}$)

$$\Omega_{\rm GW}\, h^2 = \frac{\Omega_{\rm rad}\, h^2}{2 G\, v^2\, m^2\, V} \int d\log k\, k^3 \left\langle \Lambda_{ij,lm}(\hat{\mathbf{k}}) \dot{u}_{ij}(t, \mathbf{k}) \dot{u}^*_{lm}(t, \mathbf{k}) \right\rangle_{4\pi} \tag{26}$$

which has assumed that all the vacuum energy ρ_0 gets converted into radiation, an approximation which is always valid in generic hybrid inflation models with $v \ll M_P$, and thus $H \ll m = \sqrt{\lambda}\, v$.

We have shown in Fig. 1 the evolution in time of the fraction of energy density in GW. The first (tachyonic) stage is clearly visible, with a (logarithmic) slope twice that of the anisotropic tensor Π_{ij}. Then there is a small plateau corresponding to the production of GW from bubble collisions; and finally
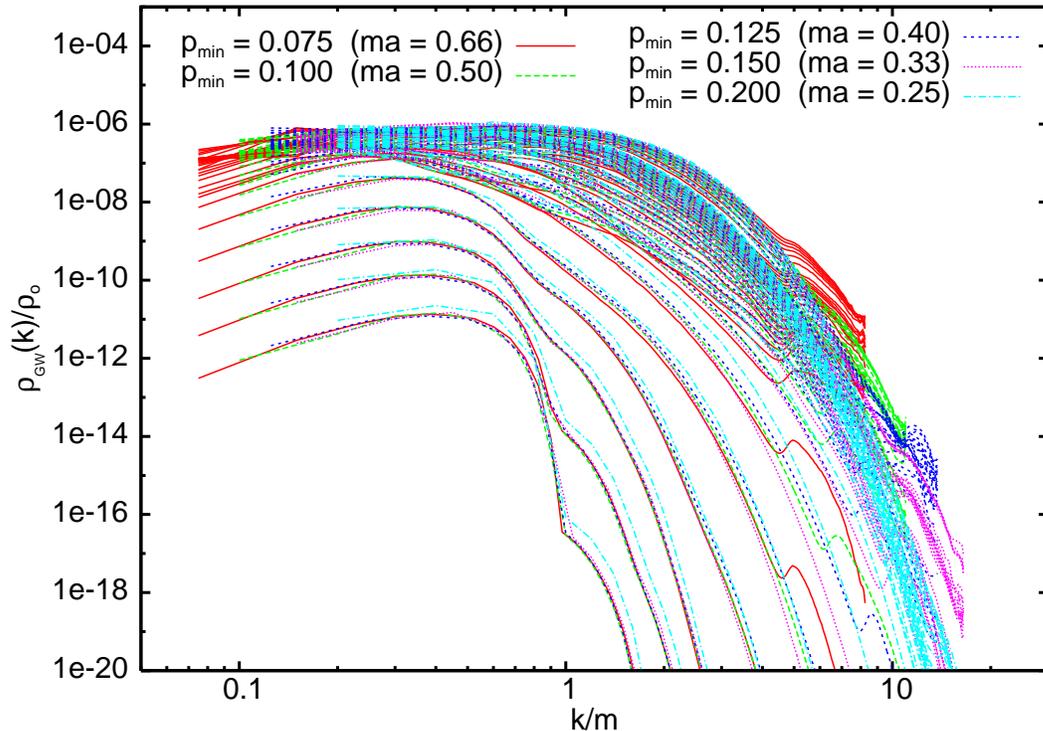
7

Figure 2: We show here the comparison between the power spectrum of gravitational waves obtained with increasing lattice resolution, to prove the robustness of our method. The different realizations are characterized by the the minimum lattice momentum (p_{min}) and the lattice spacing (ma). The growth is shown in steps of $m\Delta t = 1$ up to $mt = 30$, and then in and $m\Delta t = 5$ steps up to $mt = 60$.

there is the slow growth due to turbulence. In the next section we will describe in detail the most significant features appearing at each stage.

Note that in the case that $H \ll m$, the maximal production of GW occurs in less than a Hubble time, soon after symmetry breaking, while turbulence lasts several decades in time units of m^{-1}. Therefore, we can safely ignore the dilution due to the Hubble expansion, up to times much greater than those of the tachyonic instability. Eventually the universe reheats and the energy in gravitational waves redshifts like radiation thereafter.

To compute the power spectrum per logarithmic frequency interval in GW, $\Omega_{GW}(f)$, we just have to use (18). We can evaluate the power spectrum today from that obtained at reheating by converting the wavenumber k into frequency f. Simply using Eq. (20), with $g_{r,s}/g_{0,s} \sim 100$, $g_{r,s} \sim g_r$ and $a_e \sim a_*$, then

$$f = 6 \times 10^{10} \text{ Hz} \frac{k}{\sqrt{H M_p}} = 5 \times 10^{10} \text{ Hz} \frac{k}{m} \lambda^{1/4} . \tag{27}$$

We show in Fig. 2 the power spectrum of gravitational waves as a function of (comoving) wavenumber k/m. We have used different lattices in order to have lattice artifacts under control, specially at late times and high wavenumbers. We made sure by the choice of lattice size and spacing (i.e. k_{min} and k_{max}) that all relevant scales fitted within the simulation. Note, however, that the lower bumps are lattice artifacts, due to the physical cutoff imposed at the initial condition, that rapidly disappear with time. We have also checked that the power spectrum of the scalar fields follows turbulent scaling after $mt \sim \mathcal{O}(100)$, and we can thus estimate the subsequent evolution of the energy density distributions beyond our simulations.

3 Lattice simulations

The problem of determining the time evolution of a quantum field theory is an outstandingly difficult problem. In some cases only a few degrees of freedom are relevant or else perturbative techniques are

applicable. However, in our particular case, our interests are focused on processes which are necessarily non-linear and non-perturbative and involve many degrees of freedom. The presence of gravitational fields just contributes with more degrees of freedom, but does not complicate matters significantly.

In the present paper we will use the so called classical approximation to deal with the problem. It consists of replacing the quantum evolution of the system by its classical evolution, for which there are feasible numerical methods available. The quantum nature of the problem remains in the stochastic character of the initial conditions. This approximation has been used with great success by several groups in the past [34, 24]. The advantage of the method is that it is fully non-linear and non-perturbative.

Our approach is to discretize the classical equations of motion of all fields in both space and time. The time-like lattice spacing a_t must be smaller than the spatial one a_s for the stability of the discretized equations. In addition to the ultraviolet cut-off one must introduce an infrared cut-off by putting the system in a box with periodic boundary conditions. In this paper we have thouroughly studied a model with $g^2 = 2\lambda = 1/4$, but we have checked that other values of the parameters do not change our results significantly.

3.1 Initial conditions

The initial conditions of the fields follow the prescription from Ref. [25]. The Higgs modes ϕ_k are solutions of the coupled evolution equations, which can be rewritten as $\phi_k'' + (k^2 - \tau)\phi_k = 0$, with $\tau = M(t - t_c)$ and $M = (2V)^{1/3}m$. The time-dependent Higgs mass follows from the initial inflaton field homogeneous component, $\chi_0(t_i) = \chi_c(1 - Vm(t_i - t_c))$ and $\dot\chi_0(t_i) = -\chi_c Vm$. The Higgs modes with $k/M > \sqrt{\tau_i}$ are set to zero, while the rest are determined by a Gaussian random field of zero mean distributed according to the Rayleigh distribution

$$P(|\phi_k|)d|\phi_k|d\theta_k = \exp\left(-\frac{|\phi_k|^2}{\sigma_k^2}\right)\frac{d|\phi_k|^2}{\sigma_k^2}\frac{d\theta_k}{2\pi} , \tag{28}$$

with a uniform random phase $\theta_k \in [0, 2\pi]$ and dispersion given by $\sigma_k^2 \equiv |f_k|^2 = P(k, \tau_i)/k^3$, where $P(k, \tau_i)$ is the power spectrum of the initial Higgs quantum fluctuations, computed in the linear approximation in the background of the homogeneous inflaton. In the classical limit, the conjugate momentum $\dot\phi_k(\tau)$ is uniquely determined as $\dot\phi_k(\tau) = F(k, \tau)\phi_k(\tau)$, with $F(k, \tau) = \text{Im}(if_k(\tau)\dot f_k^*(\tau))/|f_k(\tau)|^2$, see Ref. [25].

The rest of the fields (the inflaton non-zero modes and the gravitational waves), are supposed to start from the vacuum, and therefore they are semiclassically set to zero initially in the simulations. Their coupling to the Higgs modes will drive their evolution, giving rise to a rapid (exponential) growth of the GW and inflaton modes. Their subsequent non-linear evolution will be well described by the lattice simulations. In the next subsections we will describe the different evolution stages found in our simulations.

3.2 Tachyonic growth

In this subsection we will compare the analytical estimates with our numerical simulations for the initial tachyonic growth of the Higgs modes and the subsequent growth of gravitational waves. The first check is that the Higgs modes grow according to Ref. [25]. There we found that

$$k|\phi_k(t)|^2 \simeq v^2 A(\tau) e^{-B(\tau)k^2} , \tag{29}$$

with $A(\tau)$ and $B(\tau)$ are given, for $\tau > 1$, as $A(\tau) = \frac{\pi^2 (1/3)^{2/3}}{2\Gamma^2(1/3)}\text{Bi}^2(\tau)$, and $B(\tau) = 2(\sqrt\tau - 1)$, where $\text{Bi}(z)$ is the Airy function of the second kind. We have checked that the initial growth, from $mt = 6$ to $mt = 10$, follows precisely the analytical expression.

The comparison between the tensor modes $h_{ij}(k, t)$ and the numerical results is somewhat more complicated. We should first compute the effective anisotropic tensor $T_{ij}(\mathbf{k}, t)$ (14) from the gradients of the Higgs field (those of the inflaton are not relevant during the tachyonic growth), as follows,

$$\tilde\Pi_{ij}(\mathbf{k}, t) = \int \frac{d^3\mathbf{x}\, e^{-i\mathbf{kx}}}{(2\pi)^{3/2}} [\nabla_i\phi^a \nabla_j\phi^a(\mathbf{x}, t)] , \tag{30}$$

where $\nabla_i \phi^a(\mathbf{x}, t) = \int \frac{d^3\mathbf{q}}{(2\pi)^{3/2}} i q_i \, \tilde{\phi}^a(\mathbf{q}, t) \, e^{-i\mathbf{q}\mathbf{x}}$. After performing the integral in $\mathbf{x}$ and using the delta function to eliminate $\mathbf{q}'$, we make a change of variables $\mathbf{q} \rightarrow \mathbf{q} + \mathbf{k}/2$, and integrate over $\mathbf{q}$. Finally, with the use of $\tilde{\Pi}_{ij}(\mathbf{k}, t)$, we can compute the tensor fields,

$$h_{ij}(\mathbf{k}, t) = (16\pi G) \int_0^t dt' \, \frac{\sin k(t - t')}{k} \, \tilde{\Pi}_{ij}, \qquad \partial_0 h_{ij}(\mathbf{k}, t) = (16\pi G) \int_0^t dt' \, \cos k(t - t') \, \tilde{\Pi}_{ij}. \qquad (31)$$

Using the analytic solutions one can perform the integrals and obtain expressions that agree surprisingly well with the numerical estimates. This allows one to compute the density in gravitational waves, ρ_{GW}, at least during the initial tachyonic stage in terms of analytical functions, and we reproduce the numerical results. We will now compare these with the analytical estimates. The tachyonic growth is dominated by the faster-than-exponential growth of the Higgs modes towards the true vacuum. The (traceless) anisotropic strees tensor Π_{ij} grows rapidly to a value of order $k^2 |\phi|^2 \sim 10^{-3} \, m^2 v^2$, which gives a tensor perturbation

$$\left| h_{ij} h^{ij} \right|^{1/2} \sim 16\pi G v^2 (m\Delta t)^2 10^{-3} \,, \qquad (32)$$

and an energy density in GW,

$$\rho_{\mathrm{GW}}/\rho_0 \sim 64\pi G v^2 \, (m\Delta t)^2 10^{-6} \sim G v^2 \,, \qquad (33)$$

for $m\Delta t \sim 16$. In the case at hand, with $v = 10^{-3} \, M_P$, we find $\rho_{\mathrm{GW}}/\rho_0 \sim 10^{-6}$ at symmetry breaking, which coincides with the numerical simulations at that time, see Fig. 1.

As shown in Ref. [25], the spinodal instabilities grow following the statistics of a Gaussian random field, and therefore one can use the formalism of [41] to estimate the number of peaks or lumps in the Higgs spatial distribution just before symmetry breaking. As we will discuss in the next section, these lumps will give rise via non-linear growth to lump invagination and the formation of bubble-like structures with large density gradients, expanding at the relativistic speeds and colliding among themselves giving rise to a large GWB. The size of the bubbles upon collision is essentially determined by the distance between peaks at the time of symmetry breaking, but this can be computed directly from the analysis of Gaussian random fields, as performed in Ref. [25]. This analysis works only for the initial (linear) stage before symmetry breaking. Nevertheless, we expect the results to extrapolate to later times since once a bubble is formed around a peak, it remains there at a fixed distance from other bubbles. This will give us an idea of the size of the bubbles at the time of collision.

3.3 Bubble collisions

The production of gravitational waves in the next stage proceeds through 'bubble' collisions. In Ref. [24] we showed that during the symetry breaking, the Higgs field develops lumps whose peaks grow up to a maximum value $|\phi|_{\mathrm{max}}/v = 4/3$, and then decrease creating approximately spherically symmetric bubbles, with ridges that remain above $|\phi| = v$. Finally, neighboring bubbles collide and high momentum modes are induced via field inhomogeneities. Since initially only the Higgs field sources the anisotropic stress-tensor Π_{ij}, then we expect the formation of structures in the spatial distribution of the GW energy density correlated with the Higgs lumps. In this sub-section we will give an estimate of the burst in GW produced by the first collisions of the Higgs bubble-like structures.

As for the collision of vaccum bubbles in first order phase transitions [9], we can give a simple estimate of the order of magnitude of the energy fraction radiated in the form of gravitational waves when two Higgs bubble-like structures collide. A similar stimation is indeed presented in [42, 22]. In general, the problem of two colliding bubbles has several time and length scales: the duration of the collision, Δt; the bubbles' radius R at the moment of the collision; and the relative speed of the bubble walls. The typical size of bubbles upon collisions, is of the order of $R \approx 10 m^{-1}$, while the growth of the bubble's wall is relativistic, see Ref. [25]. Then we can assume than the time scale associated with bubble collisions is also $\Delta t \sim R$. Assuming the bubble walls contain most of the energy density, it is expected that the asymmetric collisions will copiously produce GW.

Far from a source that produces gravitational radiation, the dominat contribution to the amplitude of GW is given by the acceleration of the quadrupole moment of the Higgs field distribution. Given the

energy density of the Higgs field, ρ_H, we can compute the (reduced) quadrupole moment of the Higgs field spatial distribution, $Q_{ij} = \int d^3x \, (x_i x_j - x^2 \delta_{ij}/3) \, \rho_H(x)$, such that the amplitude of the gravitational radiation, in the TT gauge, is given by $h_{ij} \sim (2G/r) \ddot{Q}_{ij}$. A significant amount of energy can be emitted in the form of gravitational radiation whenever the quadrupole moment changes significantly fast: through the bubble collisions in this case. The power carried by these waves can be obtained via (17) as

$$P_{\mathrm{GW}} = \frac{G}{8\pi} \int d\Omega \, \left\langle \dddot{Q}_{ij} \dddot{Q}^{ij} \right\rangle . \tag{34}$$

Omitting indices for simplicity, as the power emitted in gravitational waves in the quadrupole approximation is of order $P_{\mathrm{GW}} \sim G(\dddot{Q})^2$, while the quadrupole moment is of order $Q \sim R^5 \rho_H$, we can estimate the power emitted in GW upon the collision of two Higgs bubbles as

$$P_{\mathrm{GW}} \sim G \left(\frac{R^5 \rho}{R^3} \right)^2 \sim G \rho_H^2 \, R^4 \tag{35}$$

The fraction of energy density carried by these waves, $\rho_{\mathrm{GW}} \sim P_{\mathrm{GW}} \Delta t / R^3 \sim P_{\mathrm{GW}}/R^2 \sim G\rho_H^2 R^2$, compared to that of the initial energy stored in the two bubble-like structures of the Higgs field, will be $\rho_{\mathrm{GW}}/\rho_H = G\rho_H R^2$. Since the expansion of the universe is negligible during the bubble collision stage, the energy that drives inflation, $\rho_0 \sim m^2 v^2$, is transferred essentially to the Higgs modes during preheating, within an order of magnitude, see Fig. 1. Thus, recalling that $R \sim 10 m^{-1}$, the total fraction of energy in GW produced during the bubble collisions to that stored in the Higgs lumps formed at symmetry breaking, is given by

$$\frac{\rho_{\mathrm{GW}}}{\rho_0} \sim 0.1 \, G \rho_0 \, R^2 \sim (v/M_p)^2 , \tag{36}$$

giving an amplitude which is of the same order as is observed in the numerical simulations, see Fig. 1. Of course, an exhaustive analytical treatment of the production of GW during this stage of bubble collisions remains to be done, but we leave it for a future publication.

3.4 Turbulence

The development of a turbulent stage is expected from the point of view of classical fields, as turbulence usually appears whenever there exists an active (stationary) source of energy localized at some scale k_{in} in Fourier space. The oscillating inflaton zero-mode plays the role of the pumping-energy source, acting at a well defined scale k_{in} in Fourier space, given by the frequency of the inflaton oscillations. Apart from k_{in}, there is no other scale in Fourier space where energy is accummulated, dissipated and/or infused. So, as turbulence is characterized by the transport of some conserved quantity, energy in our case, we should expect a flow of energy from k_{in} towards higher (direct cascade) or smaller (inverse cascade) momentum modes. In typical turbulent regimes of classical fluids, there exits a sink in Fourier space, corresponding to that scale at which the (direct) cascade stops and energy gets dissipated. However, in our problem there is no such sink so that the transported energy cannot be dissipated, but instead it is used to populate high-momentum modes. For the problem at hand, there exists a natural initial cut-off $k_{\mathrm{out}} \sim \lambda^{1/2} v$, such that only long wave modes within $k < k_{\mathrm{out}}$, develop the spinodal instability. Eventually, after the tachyonic growth has ended and the first Higgs' bubble-like structures have collided, the turbulent regime is established. Then the energy flows from small to greater scales in Fourier space, which translates into the increase of k_{out} in time.

When the turbulence has been fully established, if the wave (kinetic) turbulence regime of the fields' dynamics is valid, the time evolution of the variance of a turbulent field $f(\mathbf{x}, t)$, should follow a power-law-like scaling [43]

$$\mathrm{Var}(f(t)) = \left\langle f(t)^2 \right\rangle - \left\langle f(t) \right\rangle^2 \propto \, t^{-2p} , \tag{37}$$

with $p = 1/(2N - 1)$ and N the number of scattering fields in a 'point-like collision'. In Fig. 3 we have plotted the time evolution of the variances of the Inflaton χ and of the Higgs modulus $\phi = \sqrt{\sum_a \phi_a^2}$, and fitted the data with a power-law like (37), obtaining
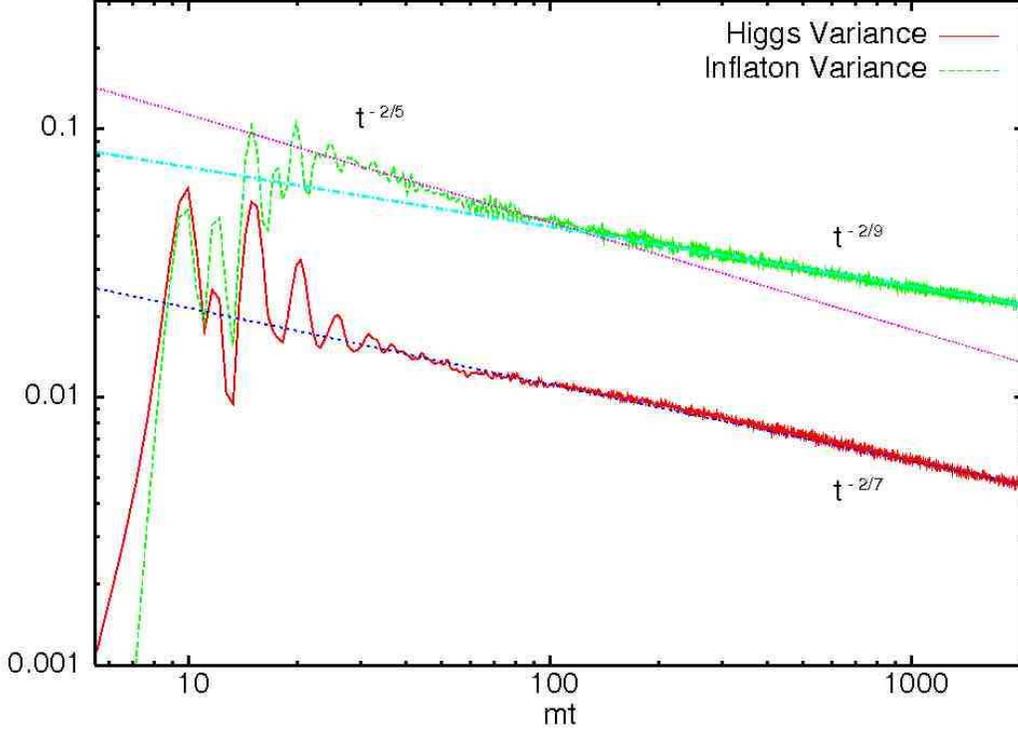
11

Figure 3: Variance of the Inflaton and the Higgs field as a function of time, the former normalized to its critical value, the latter normalized to its *v.e.v.*. As expected in a turbulent regime, these variances follow a power law $\sim t^{-2p}$ with p a certain critical exponent, although the slope of the Inflaton's variances evolves in time. The curves are produced from an average over 10 different statistical realizations.

$$\begin{aligned}
\text{Inflaton:} \quad & p_I^{-1} = 5.1 \pm 0.2, \quad && [35{:}85] \\
\text{Inflaton:} \quad & p_I^{-1} = 9.03 \pm 0.03, \quad && [350{:}2000] \\
\text{Higgs:} \quad & p_H^{-1} = 7.02 \pm 0.01, \quad && [50{:}2000]
\end{aligned}$$

where the last brackets on the right correspond to the range in time (in units of m^{-1}) for which we fitted the data. As can be seen in Fig. 3, the slope of the Higgs field (in logarithmic scale), $2p_H \sim 2/7$, remains approximately constant in time, corresponding to a 4-field dominant interaction. However, the slope of the Inflaton's variance increases in time, i.e. the critical exponent p_I of the Inflaton decreases, until it reaches a stationary stage at $mt \sim 100$. We will not try to explain here the origin of such an effective critical exponents as extracted from the simulations. We will just stress that we have checked the robustness of those values under different lattice configurations $(N, p_{\min})$ and different statistical realizations. Actually, when turbulence has fully developed, it is expected that the distribution function of the classical turbulent fields, the inflaton and the Higgs here, follow a self-similar evolution [43]

$$n(k,t) = t^{-\gamma p} n_0(k\, t^{-p}), \tag{38}$$

with p the critical exponent of the fields' variances and γ a certain factor $\sim O(1)$, which depends on the type of turbulence developed. Looking at (38), we see that the exponent p determines the speed of the particles' distribution in momentum space: given a specific scale k_c that scale evolves in time as $k_c(t) = k_c(t_0)(t/t_0)^p$. In the simulations, we have seen that the evolution of the Higgs occupation number follows Eq. (38) with $p \approx 1/7$, as expected from the Higgs variance, and $\gamma \approx 2.7$. Whereas the evolution of the Inflaton occupation number follows (38) even more accurately than the Higgs, with an "effective" exponent (once the asymptotic regime is achieved) $p \approx 1/5$, and $\gamma \approx 3.9$. In Figs. 4 we have plotted the occupation numbers of the Higgs and the Inflaton, also inverting the relation of Eq. (38) in order to extract the *universal* time-independent $n_0(k)$ functions of each field. As shown in those figures,
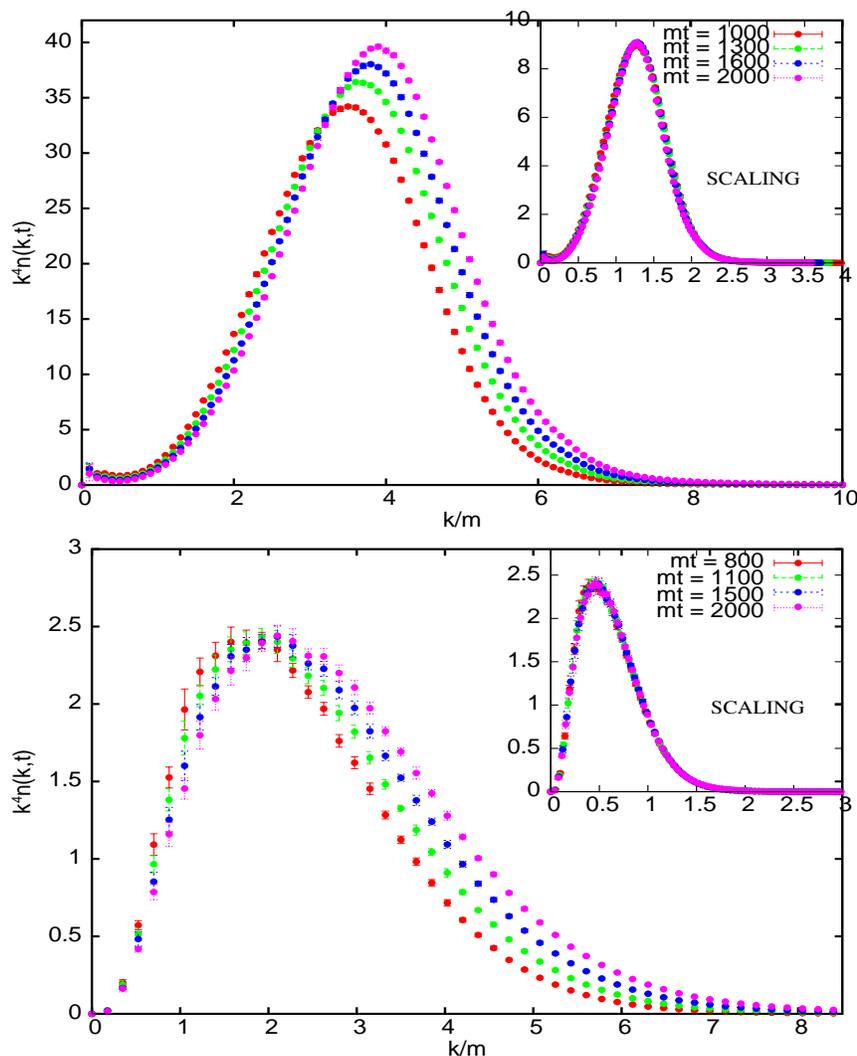
Figure 4: Some snapshots of the evolution of the spectral particle occupation numbers of the Higgs and the Inflaton fields at different times, each averaged over 10 statistical realizations. We multiply them by k^4 so we can see better the scaling behaviour. In the upper right corner, we plot the inverse relation of (38), $n_0(kt^{-p}) = t^{\gamma p}n(k,t)$, also averaged over 10 realizations for each time. The scaling behaviour predicted by wave kinetic turbulent theory [43], is clearly verified.

the distributions follow nicely the expected scaling behaviour. The universal functions $n_0(k)$ plotted in Figs. 4 have been obtained from averaging over ten statistical realizations for each time.

The advantage of the development of a turbulence behaviour is obvious: it allows us to extrapolate the time evolution of the fields' distributions till later times beyond the one we can reach with the simulations. Moreover, the fact that the turbulence develops so early after the tachyonic instability, also allow us to check for a long time of the simulation, the goodness of the description of the dynamics of the fields, given by the turbulent kinetic theory developed in Ref. [43]. We have fitted the averaged universal functions $n_0(k)$ with expressions of the form $k^4 n_0(k) = P(k)e^{-Q(k)}$, with $P(k)$ and $Q(k)$ polynomials in k. There is no fundamental meaning associated with such a fit, but it is very useful to have an analytical control over $n_0(k)$, since this allows us to track the time-evolution of $n(k,t)$ through Eq. (38). Actually, the classical regime of the evolution of some bosonic fields ends when the system can be relaxed to the Bose-Einstein distribution. Since we cannot reach that moment, we can at least estimate the moment in which the initial energy density gets fully transferred to the Higgs classical modes. Using Eq.(38) and the fit to the universal $n_0(k)$ of the Higgs, we find that the initial energy density is totally transfered to
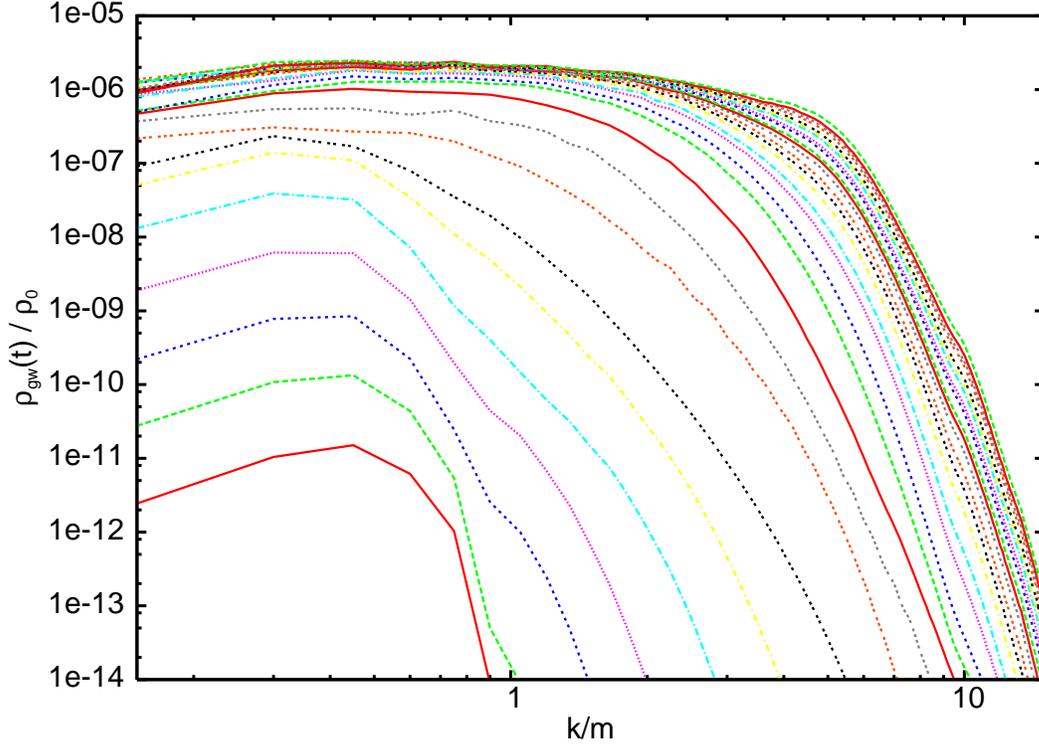
Figure 5: Time evolution of the GW spectra from mt $= 6$ to mt $= 2000$. The amplitude of the spectra seems to saturate after mt ~ 100, although the high momentum tail still moves slowly to higher values of k during the turbulent stage.

the Higgs when (in units $m = 1$)

$$\rho_0 = \frac{1}{4\lambda} = \int \frac{dk}{k} \frac{k^3}{2\pi^2} \, k \, n(k,t) = \frac{7.565}{2\pi^2} \, t^{(4-\gamma)p} \,, \tag{39}$$

where we have assumed that the Higgs' modes have energy $E_k(k,t) = k \, n(k,t)$. In our case, with $\lambda = 1/8$, the conversion of the initial energy density into Higgs particles and therefore into radiation is complete by $t \sim 6 \times 10^4 m^{-1}$. Therefore, if we consider this value as a lower bound for the time that classical turbulence requires to end, we see that turbulence last for a very long time compared to the time-scale of the initial tachyonic and bubbly stages. Thus, if GW were significatively sourced during turbulence, one should take into account corrections from the expansion of the universe.

In Fig. 5, we show the evolution of the GW spectra up to times mt $= 2000$, for a lattice of $(N, p_{\min})$ $= (128, 0.15)$. It is clear from that figure that the amplitude of the GW saturates to a value of order $\rho_{\mathrm{GW}}/\rho_0 \approx 2 \cdot 10^{-6}$. At mt ≈ 50, the maximum amplitude of the spectra has already reached $\rho_{\mathrm{GW}}/\rho_0 \approx 10^{-6}$, while at time mt ≈ 100, the maximum has only grown a factor of 2 with respect to mt ≈ 50. From times mt ≈ 150 till the maximum time we reached in the simulations, mt $= 2000$, the maximum of the amplitude of the spectrum does not seem to change significantly, slowly increasing from $\approx 2 \cdot 10^{-6}$ to $\approx 2.5 \cdot 10^{-6}$. Despite this saturation, we see in the simulations that the long momentum tail of the spectrum keeps moving towards greater values. This displacement is precisely what one would expect from turbulence, although it is clear that the amplitude of the new high momentum modes never exceed that of lower momentum. In order to disscard that this displacement towards the UV is not a numerical artefact, one should further investigate the role played by the turbulent scalar fields as a source of GW. Here, we just want to remark that the turbulent motions of the scalar fields, seem not to increase significatively anymore the total amplitude of the GW spectrum. Indeed, in a recent paper [22] where GW production at reheating is also considered, it is stated that GW production from turbulent motion of classical scalar fields, should be very supressed. That is apparently what we observe in our simulations although, as pointed above, this issue should be investigated in a more detailed way. Anyway, here we can conclude

that the expansion of the Universe during reheating in these hybrid models, does not play an important role during the time of GW production, and therefore we can be safely ignore it.

4 Gravitational Waves from Chaotic Inflation

The production of a relic GWB at reheating was first addressed by Khlebnikov and Tkachev (KT) in Ref. [18], both for the quadratic and quartic chaotic inflation scenarios. Recently, chaotic scenarios were revisited in Ref. [20, 21]. Also very recently, Ref. [22] studied in a very detail way, the evolution of GW produced at preheating in the case of a massless inflaton with an extra scalar field.

In Refs. [18] and [20], the procedure to compute the GW from reheating relied on Weinberg's formula for flat space-time [45]. However, in chaotic models, the expansion of the universe cannot be neglected during reheating, so Weinberg's formula can only be used in an approximated way, if the evolution of the universe is considered as an adiabatic sequence of stationary universes. In Ref. [17], however, we adopted a different approach that takes into account the expansion of the universe in a self-consistent manner, and allows us to calculate at any time the energy density and power spectra of the GW produced at reheating (see section 2). Using our technique, we will show in this section that we reproduce, for specific chaotic models, similar results to those of other authors. In particular, we adapted the publicly available LATTICEEASY code [31], taking advantage of the structure of the code itself, incorparating the evolution of Eq. (7), together with the equations of the scalar fields, Eqs. (4), into the staggered leapfrog integrator routine.

Here we will concentrate only in an scenario with a massless inflaton χ, either accompanied or not by an extra scalar field ϕ. Such scenarios are described by the potential

$$V(\chi, \phi) = \frac{\lambda}{4}\chi^4 + \frac{1}{2}g^2\chi^2\phi^2 \tag{40}$$

Rescaling the time by and the physical fields by a conformal transformation as

$$\chi_c(\tau) = \frac{a(\tau)}{a(0)}\frac{\chi(\tau)}{\chi(0)}, \qquad \phi_c(\tau) = \frac{a(\tau)}{a(0)}\frac{\phi(\tau)}{\chi(0)}, \qquad d\tau = \frac{a(\tau)}{a(0)}\chi(0)\sqrt{\lambda}\,dt\,, \tag{41}$$

then the equations of motion of the inflaton and of the extra scalar field, Eq. (4), can be rewritten in terms of the conformal variables as

$$\chi_c'' - \nabla^2\chi_c - \frac{a''}{a}\chi_c + (\chi_c^2 + q\phi_c^2)\chi_c = 0 \tag{42}$$

$$\phi_c'' - \nabla^2\phi_c - \frac{a''}{a}\chi_c + q\chi_c^2\phi_c = 0\,, \tag{43}$$

where the prime denotes derivative with respect to conformal time. Since the universe expands as radiation-like in these scenarios, $a(\tau) \sim \tau$, so the terms proportional to a''/a in Eqs. (42) and (43) are soon negligible, as explicitly checked in the simulations. Thanks to this, the model is conformal to Minkowski.

The parameter $q \equiv g^2/\lambda$ controls the strength and width of the resonance. For the case of a massless inflaton without an extra scalar field, we just set $q = 0$ in Eq. (42) and ignore Eq. (43). However, in that case, fluctuations of the inflaton also grow via parametric resonance. Actually, they grow as if they were fluctuations of a scalar field coupled to the zero-mode of the inflaton with effective couplig $q = g^2/\lambda = 3$, see Ref. [46]. Following Refs. [18] and [20], we set $\lambda = 10^{-14}$ and $q = 120$. Since this case is also computed in [22], we can also compare our results with theirs. Moreover, we also present results for the pure $\lambda\chi^4$ model with no extra scalar field, a case only shown in Ref. [18].

We begin our simulations at the end of inflation, when the homogeneous inflaton verifies $\chi_0 \approx 0.342 M_p$ and $\dot{\chi}_0 \approx 0$. We took initial quantum (conformal) fluctuations $1/\sqrt{2k}$ for all the modes up to a certain cut-off, and only added an initial zero-mode for the inflaton, $\chi_c(0) = 1$, $\chi_c(0)' = 0$. In Figs. 6 and 7, we show the evolution of Ω_{GW} during reheating, normalized to the instant density at each time step, for the coupled and the pure case, respectively. In the case with an extra scalar field, the amplitude of the GWB saturates at the end of parametric resonance, when the fields variances have been stabilized. This is the beginnig of the turbulent stage in the scalar fields, which seems not to source anymore the production of
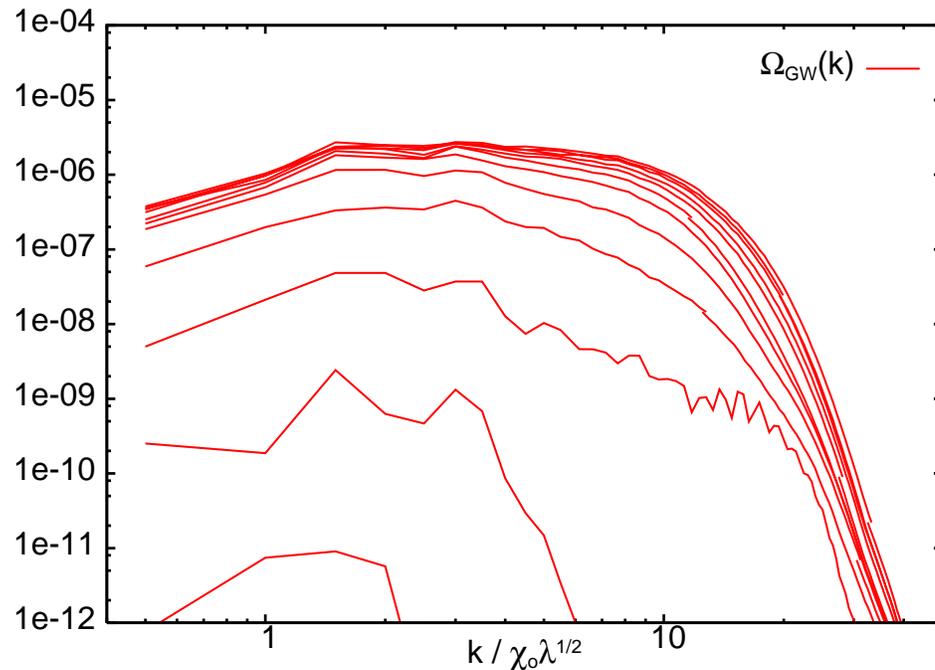
Figure 6: The spectrum of the gravitational waves' energy density, for coupled case with $\lambda = 10^{-14}$ and $g^2/\lambda = 120$. The spectrum is shown accumulated up to different times during GW production, so one can see its evolution. At each time, it is normalized to the total instant density. This plot corresponds to a N = 128 lattice simulation, from $\tau = 0$ to $\tau = 240$.

GWs, as already stated in Refs.[20, 22]. For the pure case, we also see the saturation of the amplitude of the spectra, see Fig. 7, although the high momentum tail seems to slightly move toward higher values.

Of course, in either case, with and without an extra field ϕ, in order to predict today's spectral window of the GW spectrum, we have first to normalize their energy density at the end of GW production to the total energy density at that moment; then to redshift the GW spectra from that moment of reheating, taking into account that the rate of expansion have changed significantly since the end of inflation, see Eq.(20). In particular, the shape and amplitude of GW spectra for the case with the extra scalar field coupled to the inflaton with $q = 120$, seems to coincide with the espectra shown in Ref. [22]. On the other hand, we also reproduce a similar spectra to the one shown in [18], for the case of the pure quartic model. Thanks to the tremendous gain in computer power, we were able to resolve the 'spiky' pattern of that spectrum with great resolution. For the first time, it is clearly observed the exponential tail for large frequencies, not shown in Ref. [18]. The most remarkable fact, is that we also confirm that the peak structure in the GW power spectrum, see Fig. 7, remains clearly visible at times much later than the one at which those peaks have dissapeared in the scalar fields' power spectrum. So, as pointed out in Ref. [18], this characteristic feature will allow us to distinguish this particular model from any other.

Let us emphasize that we have run the simulations till times much greater than that of the end of the resonance stage, both for the pure and the coupled case. The role of the turbulence period after preheating seems, therefore, not to be very important, despite its long duration. Apparently, the *no-go* theorem about the suppresion of GW at turbulence, discussed in [22], is fulfilled. In Refs. [27, 48] it was pointed out that gauge couplings or trilinear interactions could be responsible for a fast thermalization of the universe after inflation (see also Ref. [49]), but as long as this takes place after the end of the resonace stage, in principle this should not affect the results shown above.

5   Conclusions

To summarize, we have shown that hybrid models are very efficient generators of gravitational waves at preheating, in three well defined stages, first via the tachyonic growth of Higgs modes, whose gradients
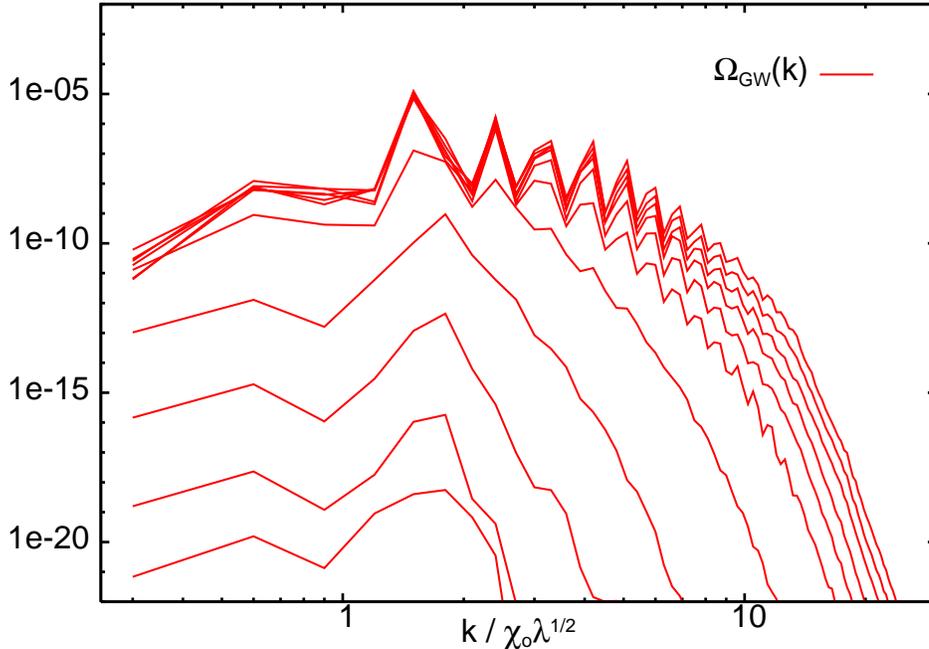
Figure 7: The spectrum of the gravitational waves' energy density, for the pure case, with $\lambda = 10^{-14}$. Again, we show the spectrum accumulated up to different times during GW production, normalized to the total instant density at each time. The plot corresponds to a N = 128 lattice simulation, from $\tau = 0$ to $\tau = 2000$.

act as sources of gravity waves; then via the collisions of highly relativistic bubble-like structures with large amounts of energy density, and finally via the turbulent regime (although this effect does not seem to be very significant in the presence of scalar sources), which drives the system towards thermalization. These waves remain decoupled since the moment of their production, and thus the predicted amplitude and shape of the gravitational wave spectrum today can be used as a probe of the reheating period in the very early universe. The characteristic spectrum can be used to distinguish between this stochastic background and others, like those arising from NS-NS and BH-BH coalescence, which are decreasing with frequency, or those arising from inflation, that are flat [50].

We have plotted in Fig. 8 the sensitivity of planned GW interferometers like LIGO, LISA and BBO, together with the present bounds from CMB anisotropies (GUT inflation), from Big Bang Nucleosynthesis (BBN) and from milisecond pulsars (ms pulsar). Also shown are the expected stochastic backgrounds of chaotic inflation models like $\lambda\phi^4$, both coupled and pure, as well as the predicted background from two different hybrid inflation models, a high-scale model, with $v = 10^{-3}M_P$ and $\lambda \sim g^2 \sim 0.1$, and a low-scale model, with $v = 10^{-5}M_P$ and $\lambda \sim g^2 \sim 10^{-14}$, corresponding to a rate of expansion $H \sim 100$ GeV. The high-scale hybrid model produces typically as much gravitational waves from preheating as the chaotic inflation models. The advantage of low-scale hybrid models of inflation is that the background produced is within reach of future GW detectors like BBO [4]. It is speculated that future high frequency laser interferometers could be sensitive to a GWB in the MHz region [12], although they are still far from the bound marked with an interrogation sign.

For a high-scale model of inflation, we may never see the predicted GW background coming from pre-heating, in spite of its large amplitude, because it appears at very high frequencies, where no detector has yet shown to be sufficiently sensitive, unless the spectrum can be extrapolated to lower frequencies, where there are interferometric detectors like BBO which could see a signal. On the other hand, if inflation occured at low scales, even though we will never have a chance to detect the GW produced during inflation in the polarization anisotropies of the CMB, we do expect gravitational waves from preheating to contribute with an important background in sensitive detectors like BBO. The detection and characterization of such a GW background, coming from the complicated and mostly unknown epoch of rehating of the universe,
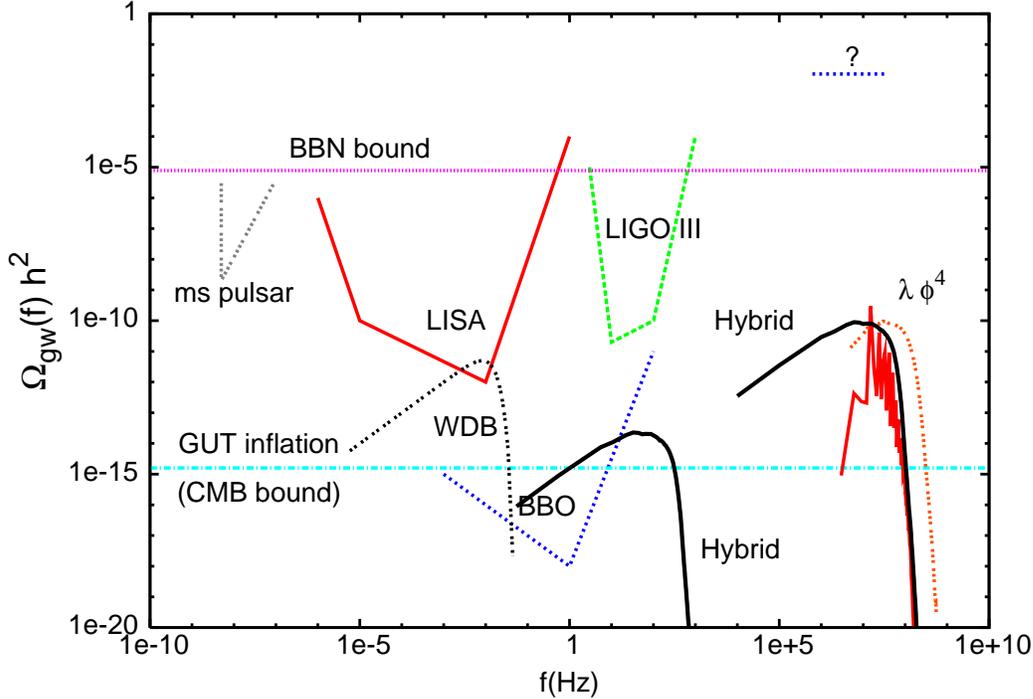
Figure 8: The sensitivity of the different gravitational wave experiments, present and future, compared with the possible stochastic backgrounds; we include the White Dwarf Binaries (WDB) [47] and chaotic preheating ($\lambda\phi^4$, coupled and pure) for comparison. Note the two well differentiated backgrounds from high-scale and low-scale hybrid inflation. The bound marked (?) is estimated from ultra high frequency laser interferometers' expectations [12].

may open a new window into the very early universe, while providing a new test on inflationary cosmology.

Acknowledgments

References

[1] M. Maggiore, Phys. Rept. **331**, 283 (2000); C. J. Hogan, arXiv:astro-ph/0608567; A. Buonanno, "Gravitational waves," arXiv:0709.4682 [gr-qc].

[2] B. Abbott *et al.* [LIGO Scientific Collaboration], Astrophys. J. **659**, 918 (2007) [arXiv:astro-ph/0608606]. LIGO Home Page: http://www.ligo.caltech.edu/

[3] S. A. Hughes, arXiv:0711.0188 [gr-qc]. LISA Home Page: http://lisa.esa.int

[4] V. Corbin and N. J. Cornish, Class. Quant. Grav. **23**, 2435 (2006); G. M. Harry, P. Fritschel, D. A. Shaddock, W. Folkner and E. S. Phinney, Class. Quant. Grav. **23**, 4887 (2006). BBO Home Page: http://universe.nasa.gov/new/program/bbo.html

[5] S. Kawamura *et al.*, Class. Quant. Grav. **23**, S125 (2006).

[6] T. L. Smith, E. Pierpaoli and M. Kamionkowski, Phys. Rev. Lett. **97**, 021301 (2006).

[7] B. Allen, gr-qc/9604033.

[8] I. H. Stairs, Living Rev. Rel. **6**, 5 (2003).

[9] A. Kosowsky, M. S. Turner and R. Watkins, Phys. Rev. Lett. **69**, 2026 (1992), Phys. Rev. D **45**, 4514 (1992); A. Kosowsky and M. S. Turner, Phys. Rev. D **47**, 4372 (1993); M. Kamionkowski, A. Kosowsky and M. S. Turner, Phys. Rev. D **49**, 2837 (1994).

[10] A. Nicolis, Class. Quant. Grav. **21**, L27 (2004); C. Grojean and G. Servant, "Gravitational waves from phase transitions at the electroweak scale and beyond," arXiv:hep-ph/0607107.

[11] A. Kosowsky, A. Mack and T. Kahniashvili, Phys. Rev. D **66**, 024030 (2002); A. D. Dolgov, D. Grasso and A. Nicolis, Phys. Rev. D **66**, 103505 (2002). G. Gogoberidze, T. Kahniashvili and A. Kosowsky, "The spectrum of gravitational radiation from primordial turbulence," arXiv:0705.1733 [astro-ph].

[12] A. Nishizawa *et al.*, "Laser-interferometric Detectors for Gravitational Wave Background at 100 MHz : Detector Design and Sensitivity," arXiv:0710.1944 [gr-qc]; A. M. Cruise and R. M. J. Ingley, Class. Quant. Grav. **23**, 6185 (2006).

[13] F. Pegoraro, L. A. Radicati, P. Bernard and E. Picasso, Phys. Lett. A **68**, 165 (1978); G. Gemme, A. Chincarini, R. Parodi, P. Bernard and E. Picasso, gr-qc/0112021; R. Ballantini *et al.*, gr-qc/0502054.

[14] A. A. Starobinsky, JETP Lett. **30**, 682 (1979) [Pisma Zh. Eksp. Teor. Fiz. **30**, 719 (1979)].

[15] L. Kofman, A. D. Linde and A. A. Starobinsky, Phys. Rev. Lett. **73**, 3195 (1994); L. Kofman, A. D. Linde and A. A. Starobinsky, Phys. Rev. D **56**, 3258 (1997).

[16] J. Garcia-Bellido and D. G. Figueroa, Phys. Rev. Lett. **98**, 061302 (2007) [arXiv:astro-ph/0701014].

[17] J. Garcia-Bellido, D. G. Figueroa and A. Sastre, "A Gravitational Wave Background from Reheating after Hybrid Inflation," arXiv:0707.0839 [hep-ph], to appear in PRD.

[18] S. Y. Khlebnikov and I. I. Tkachev, Phys. Rev. D **56**, 653 (1997).

[19] J. Garcia-Bellido, "Preheating the universe in hybrid inflation," Proceedings of the 33rd Rencontres de Moriond: Fundamental Parameters in Cosmology, Les Arcs, France, 17-24 Jan 1998, arXiv:hep-ph/9804205.

[20] R. Easther and E. A. Lim, JCAP **0604**, 010 (2006).

[21] R. Easther, J. T. . Giblin and E. A. Lim, "Gravitational Wave Production At The End Of Inflation," arXiv:astro-ph/0612294.

[22] J. F. Dufaux, A. Bergman, G. N. Felder, L. Kofman and J. P. Uzan, arXiv:0707.0875 [astro-ph].

[23] A. D. Linde, Phys. Rev. D **49**, 748 (1994); J. Garcia-Bellido and A. D. Linde, Phys. Rev. D **57**, 6075 (1998).

[24] G. N. Felder, J. Garcia-Bellido, P. B. Greene, L. Kofman, A. D. Linde and I. Tkachev, Phys. Rev. Lett. **87**, 011601 (2001); G. N. Felder, L. Kofman and A. D. Linde, Phys. Rev. D **64**, 123517 (2001).

[25] J. Garcia-Bellido, M. Garcia Perez and A. Gonzalez-Arroyo, Phys. Rev. D **67**, 103501 (2003);

[26] J. Garcia-Bellido and E. Ruiz Morales, Phys. Lett. B **536**, 193 (2002).

[27] J. Garcia-Bellido, D. Y. Grigoriev, A. Kusenko and M. E. Shaposhnikov, Phys. Rev. D **60**, 123504 (1999). J. Garcia-Bellido, M. Garcia Perez and A. Gonzalez-Arroyo, Phys. Rev. D **69**, 023504 (2004); A. Tranberg and J. Smit, JHEP **0311**, 016 (2003).

[28] A. Diaz-Gil, J. Garcia-Bellido, M. Garcia Perez and A. Gonzalez-Arroyo, PoS **LAT2005**, 242 (2006); PoS **LAT2007**, 052 (2007), arXiv:0710.0580 [hep-lat]; "Magnetic field production during preheating at the electroweak scale," arXiv:0712.4263 [hep-ph].

[29] MareNostrum Supercomputer Home Page:
http://www.bsc.es/

[30] IFT cluster Home Page:
http://lattice.ft.uam.es/iftcluster/

[31] G. N. Felder and I. Tkachev, arXiv: hep-ph/0011159;
http://www.science.smith.edu/departments/
Physics/fstaff/gfelder/latticeeasy/

[32] J. Garcia-Bellido, A. D. Linde and D. Wands, Phys. Rev. D **54**, 6040 (1996).

[33] R. Allahverdi, K. Enqvist, J. Garcia-Bellido and A. Mazumdar, Phys. Rev. Lett. **97**, 191304 (2006); R. Allahverdi, K. Enqvist, J. Garcia-Bellido, A. Jokinen and A. Mazumdar, JCAP **0706** (2007) 019 [arXiv:hep-ph/0610134].

[34] S. Y. Khlebnikov and I. I. Tkachev, Phys. Rev. Lett. **77**, 219 (1996); **79**, 1607 (1997); T. Prokopec and T. G. Roos, Phys. Rev. D **55**, 3768 (1997).

[35] V. F. Mukhanov, H. A. Feldman and R. H. Brandenberger, Phys. Rept. **215**, 203 (1992).

[36] S. Carroll, "*Spacetime and Geometry: An introduction to General Relativity,*" Addison Wesley (2003).

[37] K. G. Wilson, Phys. Rev. D **10**, 2445 (1974).

[38] F. Cooper, S. Habib, Y. Kluger, E. Mottola, J. P. Paz and P. R. Anderson, Phys. Rev. D **50**, 2848 (1994) [arXiv:hep-ph/9405352]; F. Cooper, S. Habib, Y. Kluger and E. Mottola, Phys. Rev. D **55**, 6471 (1997) [arXiv:hep-ph/9610345].

[39] D. Boyanovsky, D. Cormier, H. J. de Vega, R. Holman, A. Singh and M. Srednicki, Phys. Rev. D **56**, 1939 (1997) [arXiv:hep-ph/9703327]; D. Boyanovsky, H. J. de Vega, R. Holman and J. Salgado, Phys. Rev. D **59**, 125009 (1999) [arXiv:hep-ph/9811273].

[40] J. Baacke, K. Heitmann and C. Patzold, Phys. Rev. D **55**, 2320 (1997) [arXiv:hep-th/9608006]; Phys. Rev. D **55**, 7815 (1997) [arXiv:hep-ph/9612264]; Phys. Rev. D **56**, 6556 (1997) [arXiv:hep-ph/9706274].

[41] J. M. Bardeen, J. R. Bond, N. Kaiser and A. S. Szalay, Astrophys. J. **304**, 15 (1986).

[42] G. N. Felder and L. Kofman, Phys. Rev. D **75** (2007) 043518 [arXiv:hep-ph/0606256].

[43] R. Micha and I. I. Tkachev, Phys. Rev. Lett. **90**, 121301 (2003); Phys. Rev. D **70**, 043538 (2004).

[44] http://lattice.ft.uam.es/gw

[45] S. Weinberg, "*Gravitation and Cosmology*", John Wiley & Sons, 1972.

[46] P. B. Greene, L. Kofman, A. D. Linde and A. A. Starobinsky, Phys. Rev. D **56**, 6175 (1997) [arXiv:hep-ph/9705347].

[47] A. J. Farmer and E. S. Phinney, Mon. Not. Roy. Astron. Soc. **346**, 1197 (2003).

[48] J. F. Dufaux, G. N. Felder, L. Kofman, M. Peloso and D. Podolsky, JCAP **0607**, 006 (2006).

[49] G. N. Felder and L. Kofman, Phys. Rev. D **63**, 103503 (2001).

[50] T. L. Smith, M. Kamionkowski and A. Cooray, Phys. Rev. D **73**, 023504 (2006).